Research Article | Vol. 28, No. 9 / 27 April 2020 / Optics Express 12650
Optics EXPRESS

Solution-processed antireflective coating for back-contact perovskite solar cells

DOROTA M. BACAL,[1,2] NIRAJ N. LAL,[1,3,4] ASKHAT N. JUMABEKOV,[5,6] QICHENG HOU,[1,2] YINGHONG HU,[7] JIANFENG LU,[1] ANTHONY S. R. CHESMAN,[2,5,8] AND UDO BACH[1,2,8,*]

[1]*Department of Chemical Engineering, Monash University, Clayton, Victoria 3800, Australia*
[2]*ARC Centre of Excellence in Exciton Science, Monash University, Clayton, Victoria 3800, Australia*
[3]*First Principles Consulting, Richmond, Victoria 3121, Australia*
[4]*Centre for Sustainable Energy Systems, Australian National University, Acton, ACT 2600, Australia*
[5]*CSIRO Manufacturing, Clayton, Victoria 3168, Australia*
[6]*Department of Physics, Nazarbayev University, Nur-Sultan 010000, Kazakhstan*
[7]*Department of Chemistry and Center for NanoScience (CeNS), LMU Munich, Munich 80539, Germany*
[8]*Melbourne Centre for Nanofabrication, Clayton, Victoria 3168, Australia*
[*]*udo.bach@monash.edu*

Abstract: Back-contact architectures for perovskite solar cells eliminate parasitic-absorption losses caused by the electrode and charge collection layers but increase surface reflection due to the high refractive index mismatch at the air/perovskite interface. To mitigate this, a ~85 nm thick layer of poly(methyl methacrylate) (PMMA), with a refractive index between those of air and perovskite, has been applied as an antireflective coating. Transfer matrix modelling is used to determine the ideal PMMA layer thickness, with UV-Vis spectroscopy measurements used to confirm the increase in absorption that arises through the application of the antireflective coating. The deposition of a thin film of PMMA via spin coating onto a solar cell results in a 20–30% relative increase in short circuit current density and stable power output density.

1. Introduction

The power conversion efficiencies (PCEs) of perovskite solar cells (PSCs) have increased tremendously over the last few years [1–3], with the record PCE for a certified PSC now exceeding 25% [4]. Perovskite solar cells typically employ a planar structure in which the perovskite photoabsorber layer is sandwiched between two electrical contacts and their respective charge selective layers. While this architecture allows for ease of fabrication, efficiencies are limited due to light transmission losses caused by either reflection at material interfaces or parasitic light absorption by the transparent conducting electrode or the charge selective layers [Fig. 1(a)].

Recently, we reported a novel quasi-interdigitated back-contact (BC) architecture for PSCs [5,6], in which both electrodes are located at the base of the device [Fig. 1(b)]. This structure allows for the direct illumination of the perovskite photoabsorber layer, thus eliminating the aforementioned transmission losses. The BC configuration further permits direct in-situ measurement of the perovskite layer's optoelectronic and spectroscopic properties during film formation [7], as well as post-deposition treatments and operation. Numerical simulations performed by Ma *et al.* show that BC PSCs can theoretically obtain a higher PCE than the standard sandwich structure [8]. However, to date all reported BC PSC devices show significantly lower efficiencies than conventional planar PSCs [9–12].

In the process of improving the efficiency of BC PSCs one needs to address another potential source of light loss, namely the reflection of light by the perovskite layer that occurs due to a high refractive index mismatch between perovskite and air.

#384039 https://doi.org/10.1364/OE.384039
Journal © 2020 Received 30 Dec 2019; revised 13 Mar 2020; accepted 13 Mar 2020; published 14 Apr 2020

Optics EXPRESS

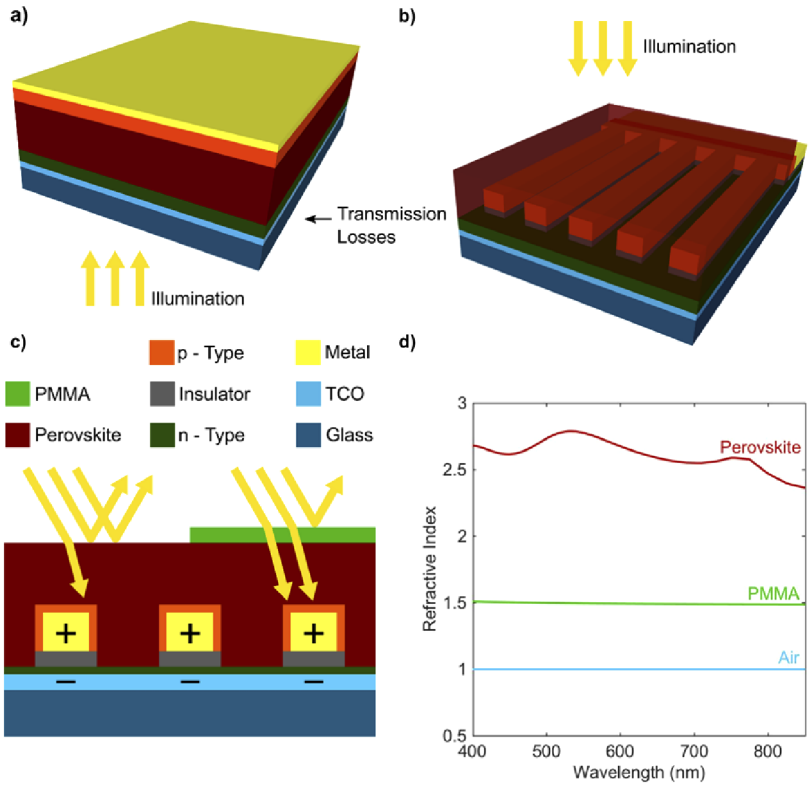

Fig. 1. Schematic cross-section diagrams of (a) planar and (b) quasi-interdigitated back-contact perovskite solar cells. TCO – transparent conductive oxide. (c) Reduced reflection from a top layer of perovskite solar cell after the deposition of the PMMA ARC. (d) Refractive index dependence on wavelength for air, PMMA [22], and perovskite (methylammonium lead iodide) [23].

The minimization of light reflectance in order to enhance the photovoltaic performance of BC solar cells, for instance in Si-based devices, has already been explored for decades. The reflection of light by the top surface of monocrystalline silicon solar cells is reduced by texturing the front of the cell with a pyramid-shaped pattern, usually through anisotropic etching in alkaline solutions [13]. However, this process is less effective for multicrystalline silicon solar cells, due to the random orientation of the crystals. Therefore, the texturing of the top surface of these devices is usually achieved through other techniques, such as reactive ion etching [14] or acidic etching [15].

Another approach to increase light absorption, typically used in conjunction with surface texturing in inorganic solar cells, is the application of an antireflective coating (ARC). This addresses the mismatch of refractive indices at the photoaborber/air interface, thus decreasing reflection at the surface of the solar cell. Due to the sensitivity of photoabsorber material, the texturing techniques typically employed in minimizing reflective losses in conventional inorganic solar cells cannot be directly transferred to hybrid organic-inorganic perovskite solar cells, leaving the application of an ARC as the only facile route to minimize reflection losses. However, conventional inorganic ARCs, such as SiN_x, SiO_x, SiO_xN_x and TiO_2 for c-Si solar cells or MgF applied to glass in sandwich perovskite solar cells, are deposited by methods that may damage the perovskite photoabsorber, leaving organic polymer coatings as viable ARC materials [16–21]. This still presents a challenge; the ARC and the solvents used in its deposition must be chemically

Optics EXPRESS

compatible with the underlying perovskite layer. One candidate is poly(methyl methacrylate) (PMMA), which has a refractive index of ~1.5 [22], which lies between the refractive indices of air and methylammonium lead iodide [23] in the visible wavelength spectrum [Figs. 1(c)–1(d)].

A layer of PMMA ARC can be deposited simply by spin coating a dilute solution of PMMA in chlorobenzene onto a perovskite film. It has been demonstrated that a PMMA layer deposited in such way has no adverse effects on the underlying perovskite layer during its use as an encapsulant in energy-dispersive X-ray [24] and surface photovoltage spectroscopy measurements [25], and in microwave photoconductivity imaging [26]. Furthermore, in 2014 Habisreutinger et al. proposed a charge selective layer made of carbon nanotubes and PMMA that sealed the perovskite layer, thus retarding moisture-related degradation processes [27,28].

Here we present theoretical and experimental investigations into the use of PMMA as an ARC for BC perovskite solar cell devices. Transfer matrix optical simulations are performed to predict the performance enhancement of the solar cells and determine the optimal thickness of the PMMA ARC. UV-Vis spectroscopic measurements are used to quantify the effect of the PMMA ARC over the different areas of the BC PSC. The device measurements confirm an increase in PCE with the use of the ARC.

2. Methods

2.1. Materials

Lead(II) iodide (99.9985%) was supplied by Alfa Aesar. Poly(methyl methacrylate) (average Mw ~996,000 by GPC), titanium diisopropoxide bis(acetylacetonate) (75 wt. % in isopropanol), N,N-dimethylformamide (anhydrous, 99.8%), chlorobenzene (anhydrous, 99.8%), dimethyl sulfoxide (anhydrous ≥99.9%), 2-propanol (anhydrous, 99.5%), lead(II) bromide (99.999%) and cesium iodide (99.999%) were supplied by Sigma-Aldrich. For cleaning, ethanol and acetone from Univar, 2-propanol (EMPARTA) from Merck and Hellmanex III from Hellma were used. FTO-coated glass was FTO-P003 (<15 ohm/sq). Methylammonium (MA) bromide and formamidinium (FA) iodide were supplied by GreatCell Solar. High-purity nitrogen (99.999%; $O_2 \leq 2$ ppm, $H_2O \leq 0.1$ ppm) was used in all operations and whenever N_2 is mentioned.

2.2. Device fabrication

Substrate Preparation: 2.5 × 2.5 cm patterned FTO-coated glass pieces were sonicated in baths of Hellmanex (1% volume concentration in water), water, and ethanol, each for 10 min, and then cleaned by an ozone plasma treatment step for 10 min. The glass pieces were then heated to 500 °C over 30 min, with this temperature then maintained for an additional 10 min to stabilize the temperature of the substrate. A TiO_2 layer was formed via the spray pyrolysis of titanium diisopropoxide bis(acetylacetonate) diluted in isopropanol (v/v 1:19). After the deposition, the temperature of the glass was maintained at 500 °C for 10 min, and then allowed to cool to room temperature while remaining on the hot plate.

Quasi-Interdigitated Electrode Fabrication: The back contact (BC) electrodes were fabricated via the photolithography method developed by us [5,6]. Prior to photoresist deposition, a thin adhesion layer of HDMS was spin coated onto the substrate for 30 s at 7000 rpm and baked for 2 min at 110 °C. Subsequently, an approximately 2 µm thick layer of AZ1512HS photoresist was spin coated using the same conditions and baked for 2 min at 110 °C. Samples were exposed to UV light (specific power 10.4 mW cm^{-2} at 365 nm) through a patterned chrome photomask, with an exposure time 7.6 s. The structure was then developed in an AZ726MIF and water solution (v/v 3:1) for approximately 1 min.

120 nm of Al_2O_3, 30 nm of Al and 50 nm of Ni were evaporated using an electron beam evaporator on top of the developed pattern. Subsequently, the photoresist was removed by sonication in acetone (lift-off process). The substrates were rinsed with isopropanol and water

Optics EXPRESS

and dried under a stream of nitrogen. The substrates were then annealed on a hotplate at 300 °C for 15 min in order to oxidise the top layer of Ni to form a NiO_x shell on top of the electrodes.

Perovskite Deposition: Prior to perovskite deposition the substrates were cleaned by an ozone plasma treatment step for 10 min and masked with Scotch tape. The perovskite precursor solution was prepared in a N_2-filled glove box by dissolving FAI (172 mg, 1 mmol), PbI_2 (507.1 mg, 1.1 mmol), MABr (23.4 mg, 0.2 mmol) and $PbBr_2$ (73.4 mg, 0.22 mmol), CsI (16.9 mg, 0.065 mmol) in 1 mL of mixed solvent of DMF:DMSO (v/v 4:1) to achieve a final composition of $Cs_{0.05}FA_{0.79}MA_{0.16}PbI_{2.49}Br_{0.51}$ with a concentration of 1.32 M. Deposition of the perovskite was achieved by spin-coating 50 µL of the precursor solution using a two-step program: 10 s at 1000 rpm (1000 rpm s^{-1} ramp) and then 20 s at 6000 rpm (6000 rpm s^{-1} ramp). 200 µL of chlorobenzene was deposited onto the spinning substrate 5 s prior to the end of the second step. The substrates were then annealed in the dark at 100 °C for 1 h and then allowed to cool to room temperature naturally. All procedures were carried out in a N_2-filled glove box.

PMMA Deposition: Poly(methyl methacrylate) was dissolved in chlorobenzene (concentration 0.1 M) by stirring overnight at 70 °C. 70 µL of the PMMA solution was spin coated at 1000 rpm for 45 s on top of the perovskite layer. All procedures were carried out in a N_2-filled glove box.

2.3. Device characterization

The J-V characteristics of the solar cells were measured under a nitrogen atmosphere with a computer-controlled Keithley 2400 Sourcemeter. The cells were illuminated with a 150 W Xenon lamp (Newport) coupled with an AM 1.5G solar spectrum filter through a quartz window. The light intensity was adjusted and monitored using a secondary reference photodiode (Hamamatsu S1133, with KG-5 filter, 2.8 × 2.4 mm of photosensitive area), calibrated by a certified reference cell (PVMeasurements, certified by NREL) under 1000 W m^{-2} AM 1.5G illumination from an Oriel AAA solar simulator fitted with a 1000 W Xenon lamp. The samples were measured through a shading mask with a photo active area of 0.015 cm^2. The voltage was changed between −0.1 and 1.1 V with an interval of 0.02 V.

Cross section SEM images of the solar cells were obtained using a Zeiss Merlin Scanning Electron Microscope with 5kV beam energy. Surface SEM images were obtained using a Nova NanoSEM 450 Scanning Electron Microscope operated at 3 kV and spot size 2.0. UV-Vis spectra of the solar cells and the separate layers were measured using a Perkin Elmer Lambda 1050 spectrometer fitted with an integrating sphere attachment in an ambient atmosphere. Diffuse reflection was determined as the total reflection with the specular reflection component removed.

3. Results and discussion

Transfer matrix (TM) optical modelling was performed for the previously reported BC PSC. For the purpose of the calculations, the anode of the quasi-interdigitated BC electrode was assumed to be a continuous layer of fluorine doped tin oxide (FTO) on a glass substrate, coated with 50 nm TiO_2. The cathode rested on the anode separated by a thin Al_2O_3 insulating layer, and was made of comb-shaped Ni coated with a thin NiO_x oxide layer. The BC PSC was completed by a thin layer of $MAPbI_3$ perovskite photoabsorber layer, covering both the anode and cathode in a conformal manner with thicknesses of 600 nm and 370 nm, respectively.

The TM modelling was performed for the device without and with a PMMA ARC over the perovskite photoabsorber. The calculations were undertaken in MATLAB with bespoke software based on the formalism of Pettersson *et al*. [29]. Figure 2(a) shows the calculated transmission and reflection spectra of the BC PSC based on literature refractive index values [22,23,30–34], without (red line) and with the PMMA ARC (green line). The absorption spectra of the perovskite photoabsorber layer in both cases were calculated through simulation of the full optical field via the Transfer Matrix method [Fig. 2(b)]. All presented graphs are a result of an average over both electrode regions.

Optics EXPRESS

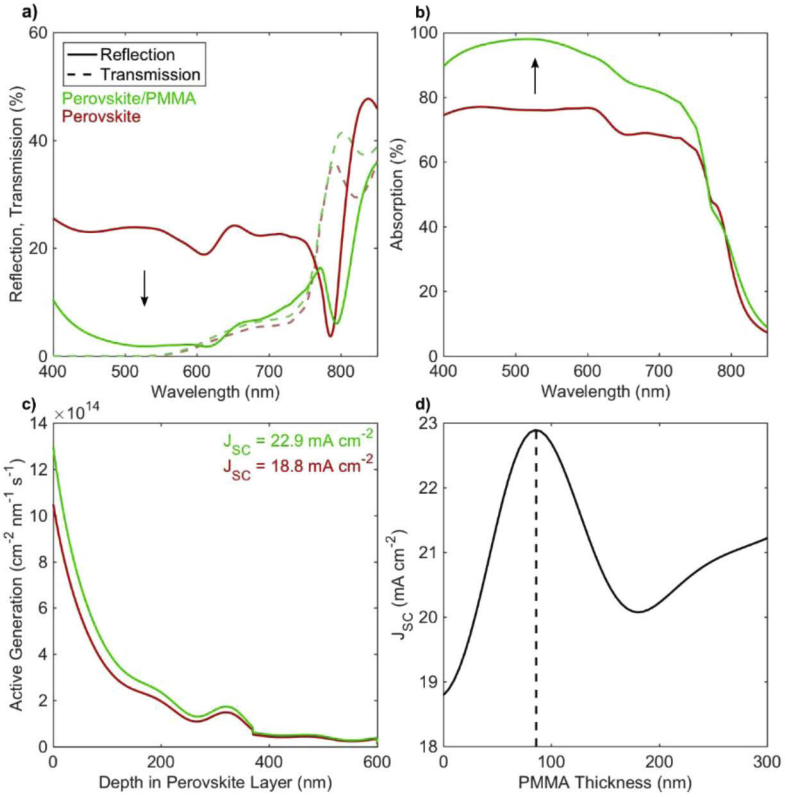

Fig. 2. Transfer matrix optical simulation of a BC PSC with (green line) and without (red line) the 85 nm thick PMMA ARC. (a) Transmission and reflection spectra based on the refractive indices data acquired from the literature, calculated as the weighted average over both contacts. (b) Calculated absorption spectra of the perovskite layer. (c) Simulated active charge carrier generation through the photoactive area of the device. (d) Calculated maximum J_{SC} value, assuming 100% charge carrier collection efficiency, as a function of PMMA thickness, with an optimum at 85 nm.

Based on the calculated absorption spectra, we estimated the maximum achievable short-circuit photocurrent density (J_{SC}) under incident AM1.5G solar irradiation to be 18.8 and 22.9 mA cm^{-2} for the device without and with a PMMA ARC, respectively. The >20% gain in photocurrent caused by the ARC results from a greater impedance matching to the absorbing perovskite layer and an increase in the photo-generation near the front of the cell [Fig. 2(c)]. The TM optical modelling revealed that such a significant increase in photocurrent can be achieved with an optimum thickness of 85 nm for the PMMA ARC [Fig. 2(d)].

As a next step, a ~400 nm thick perovskite film was characterized through UV-Vis spectroscopy measurements, with and without the PMMA ARC. Due to the small active area (2 × 2mm) of the photovoltaic devices prepared in this study, a direct optical characterization of a BC PSC could not be achieved with satisfactory accuracy. Therefore, the experiments were performed on glass substrates covered with fluorine-doped tin oxide (FTO). The thickness of the PMMA ARC layer (~85 nm) was chosen according to the results of the TM modelling.

We observed that the application of the PMMA ARC resulted in a negligible change in transmission below 750 nm wavelength. The presence of the PMMA layer caused a reduction in average reflection from ~21.5% to ~12.5% over the visible part of the spectrum (400–750 nm),

Optics EXPRESS

yielding a ~40% relative decrease in reflection [Fig. 3(a)]. This is attributed to a reduction in both specular and diffuse reflection, which suggests a random orientation of the perovskite crystals on the film surface [Fig. 3(b)]. The significant change in the optical properties of the sample resulted in ~11.5% relative increase in photo-absorption of the perovskite film, as calculated as an average over the visible component of the absorption spectra [Fig. 3(c)]. We speculate that the difference between the anticipated gain (calculated through TM modelling) and the gain observed in the acquired absorption spectra is caused by irregular coverage of the perovskite surface by the ARC due to surface roughness. However, the UV-Vis spectroscopy results clearly demonstrate that a beneficial increase in absorption can be achieved by coating PMMA onto a perovskite photoabsorber layer deposited onto a BC electrode.

In order to validate the predictions of the TM modelling, we fabricated BC PSCs and recorded their solar cell performance without and with a PMMA ARC. The SEM cross-section image of the device shows that the thickness of the PMMA ARC layer varies between 80 and 90 nm across the sample surface [Fig. 3(d)]. This is caused by the random crystal orientation of the perovskite layer deposited on top of the BC electrodes. Moreover, a top view SEM picture of the sample further reveals numerous imperfections in the perovskite film, referred to as 'pin holes' elsewhere, and the wave-shaped nature of the photoactive layer resting on the electrodes (Fig. 4).

In order to distinguish photovoltaic performance improvements resulting from the antireflective PMMA layer from those resulting from solvent exposure at the perovskite/air interface, all solar cells were tested in the following sequence: (a) BC PSC as fabricated, (b) the same device after pure chlorobenzene was spin-coated on the surface and (c) the same device after an additional spin-coating step with PMMA in chlorobenzene to apply the ARC. We observed that the neat chlorobenzene treatment only brought about very minor changes in photovoltaic performance and no noticeable difference in the UV-Vis spectra (Fig. 5). Short circuit currents (J_{SC}) and open-circuit voltages (V_{OC}) recorded in forward and reverse bias scan directions varied by less than 2% as a result of the treatment. All devices showed a strong hysteresis behavior, with a scan-direction dependent efficiency variability of more than a factor of 2. We therefore used maximum power point tracking to determine stabilized power outputs as a more meaningful estimate for the energy conversion efficiency of these solar cells.

Coating of the perovskite top surface with a thin layer of PMMA resulted in a significant improvement in the photovoltaic performance [Figs . 3(e)–3(f), Fig. 6]. Short circuit currents measured in reverse scan mode improved by ~21.5% to an average of 16.21 mA/cm^2 while stabilized power conversion efficiencies improved by ~31% to an average of 3.07%. The measured short circuit current is lower than the predicted ideal value due to the anticipated (but not modelled) recombination losses inside of the perovskite material and at the interfaces. The observed improvements in fill factors (< 6%) and open circuit voltages (4%) were only marginal.

The best performing BC PSC with a PMMA ARC exhibited a J_{SC} of 18.6 mA/cm^2 and a stabilized power output of 4.41%, which is to date the highest reported efficiency for a BC PSC with a quasi-interdigitated back-contact electrode (Fig. 7).

The relative increase in short circuit current being greater than the increase in light absorption would suggest that the application of the PMMA layer may also have a passivating effect on the surface of the perovskite layer [35–38]. In order to elucidate this effect, we performed time-resolved photoluminescence (PL) measurements on perovskite films before and after PMMA layer coating to examine the influence of the PMMA layer on carrier lifetime (Fig. 8). The results of our measurements show that PL decay for a perovskite film with a PMMA layer is considerably slower compared to the PL decay measured for the same perovskite film prior to coating with the PMMA layer. We performed fitting of the experimental time-resolved PL data with a double exponential decay function to evaluate the decay time constants τ_1 and τ_2. Fitting results show that for pristine perovskite $t_1 = 1.04 \pm 0.09$ ns and $t_2 = 777.31 \pm 13.42$ ns, whereas for a perovskite with a PMMA coating t_1 and t_2 are 4.26 ± 0.67 ns and 1616.88 ± 71.65 ns, respectively. This

Optics EXPRESS

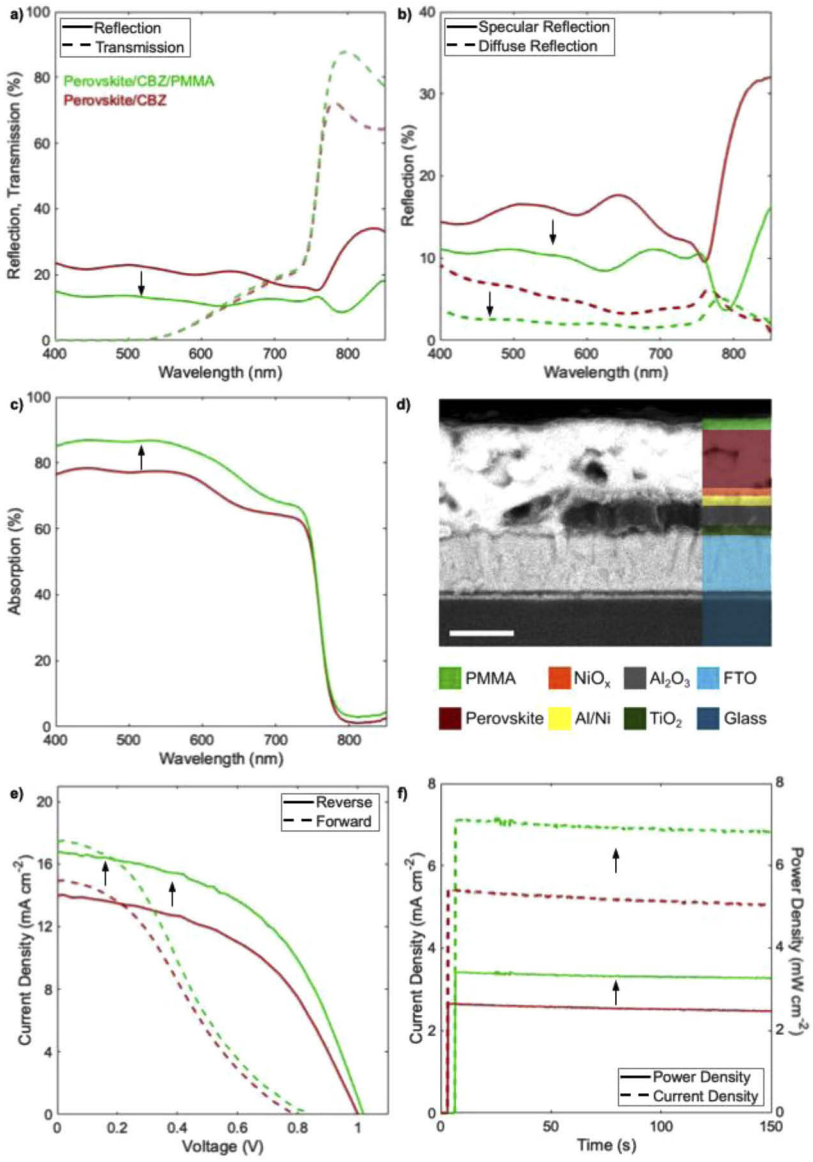

Fig. 3. (a) Transmission and reflection spectra of the perovskite layers on an FTO-coated glass substrate. (b) Calculated absorption spectra of the perovskite layers. (c) Cross-section SEM image of the back-contact perovskite solar cells covered with PMMA layer, scale bar 400 nm. (d) Typical J-V characteristic of BC PSCs under AM1.5 (1000 W/m^2) simulated solar irradiation in reverse and forward scan directions before and after the deposition of the PMMA antireflective coating. (e) Typical time evolution of stabilized maximum power output and (f) corresponding maximum power point photocurrent. Red line – samples without anti-reflective coating, green line – samples covered with the anti-reflective PMMA coating.

Optics EXPRESS

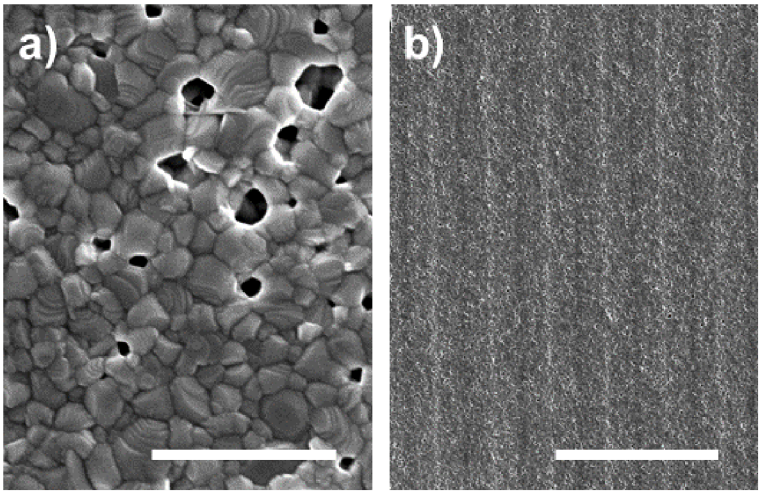

Fig. 4. (a) High magnification SEM images of perovskite layer deposited on top of BC electrodes. Scale bar 1 µm. (b) Lower magnification image of the same structure. Scale bar 10 µm.

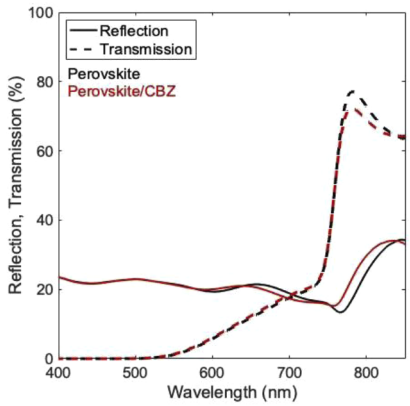

Fig. 5. Reflection and transmission spectra of a perovskite layer on Glass/FTO substrate before and after spin coating chlorobenzene on its surface.

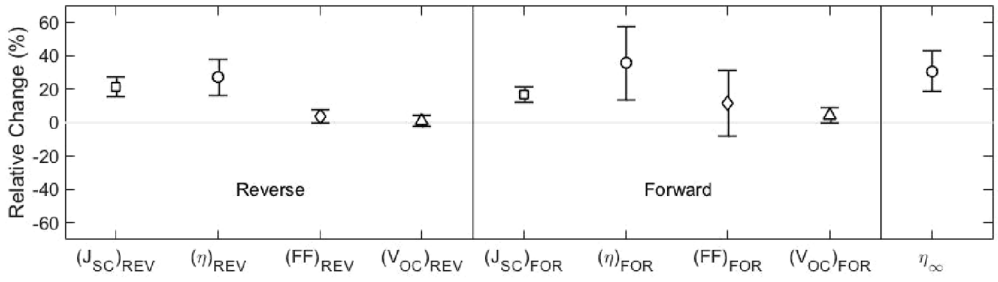

Fig. 6. Relative percentage change of solar cell parameters after the deposition of PMMA ARC. Bars show standard deviation.

Optics EXPRESS

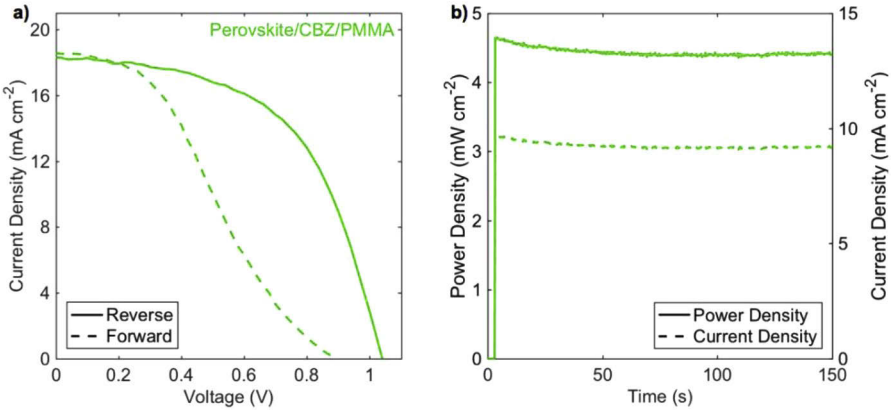

Fig. 7. (a) Current voltage characteristic of the champion BC PSC. (b) Power density and corresponding current density tracking.

indicates that the charge carriers' lifetime in perovskite films with the PMMA layer are longer when compared to neat films. Combined with the *J-V* measurements for complete devices this result suggest that the PMMA layer indeed has a passivation effect on the surface of perovskite film, although determination of the mechanism of this passivation is beyond the scope of this study.

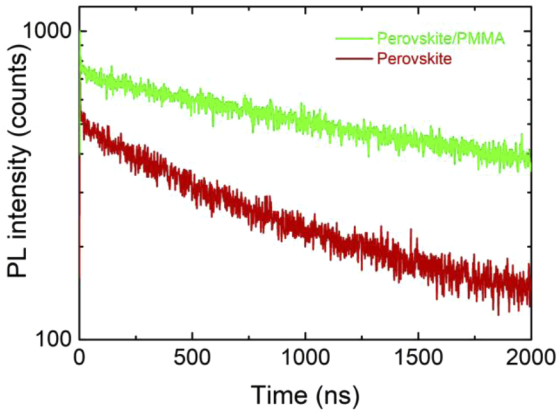

Fig. 8. Time-resolved photoluminescence (PL) spectra of a perovskite film before and after PMMA coating. The excitation wavelength of the laser was fixed at 510 nm and the PL maximum around 780 nm was monitored using time-correlated single photon counting (TCSPC).

4. Conclusion

Employing a back-contact architecture is predicted to give perovskite solar cells with efficiencies that exceed those possible with a conventional sandwich structure. However, achieving these efficiencies requires minimization of reflection at the photoabsorber/air interface. To this end, we demonstrated that PMMA makes an effective ARC on back-contact perovskite solar cells due to its optical properties, chemical compatibility with the photoabsorber material, passivating properties, and its ease of deposition. With the optimal PMMA ARC thickness determined by transfer matrix modelling, back-contact cells demonstrated an increase in photocurrent, resulting

Optics EXPRESS

in a ~30% average relative increase in the stabilized power output. This surface treatment yielded a champion solar cell with a stabilized power output of 4.41%, the highest reported for a back-contact perovskite solar cell.

Funding

Australian Research Council (CE170100026, DP160104575); Australian Centre for Advanced Photovoltaics; Australian Renewable Energy Agency; Commonwealth Scientific and Industrial Research Organisation.

Acknowledgments

This work was performed in part at the Melbourne Centre for Nanofabrication (MCN) in the Victorian Node of the Australian National Fabrication Facility (ANFF). The authors thank Dr. Ricky T. Tjeung and Dr. Yang Choon Lim for their assistance with photolithography and electron-beam evaporation. The authors thank Mark Greaves from CSIRO Manufacturing for help with SEM measurements. The authors also acknowledge use of facilities within the Monash Centre for Electron Microscopy (MCEM). The authors are also thankful to Dr. Alexander R. Pascoe for developing and optimizing the method of depositing the PMMA layer.

Disclosures

The authors declare no conflicts of interest.

References

1. J. Burschka, N. Pellet, S.-J. Moon, R. Humphry-Baker, P. Gao, M. K. Nazeeruddin, and M. Grätzel, "Sequential deposition as a route to high-performance perovskite-sensitized solar cells," Nature **499**(7458), 316–319 (2013).
2. J. H. Noh, S. H. Im, J. H. Heo, T. N. Mandal, and S. Il Seok, "Chemical Management for Colorful, Efficient, and Stable Inorganic–Organic Hybrid Nanostructured Solar Cells," Nano Lett. **13**(4), 1764–1769 (2013).
3. H. Zhou, Q. Chen, G. Li, S. Luo, T.-b. Song, H.-S. Duan, Z. Hong, J. You, Y. Liu, and Y. Yang, "Interface engineering of highly efficient perovskite solar cells," Science **345**(6196), 542–546 (2014).
4. National Renewable Energy Laboratory, "Solar cell efficiency chart," https://www.nrel.gov/pv/cell-efficiency.html. (Accessed 13 March 2020)
5. A. N. Jumabekov, E. Della Gaspera, Z.-Q. Xu, A. S. R. Chesman, J. van Embden, S. A. Bonke, Q. Bao, D. Vak, and U. Bach, "Back-contacted hybrid organic–inorganic perovskite solar cells," J. Mater. Chem. C **4**(15), 3125–3130 (2016).
6. Q. Hou, D. Bacal, A. N. Jumabekov, W. Li, Z. Wang, X. Lin, S. H. Ng, B. Tan, Q. Bao, A. S. R. Chesman, Y. B. Cheng, and U. Bach, "Back-contact perovskite solar cells with honeycomb-like charge collecting electrodes," Nano Energy **50**, 710–716 (2018).
7. M. Alsari, O. Bikondoa, J. Bishop, M. Abdi-Jalebi, L. Y. Ozer, M. Hampton, P. Thompson, M. T. Hörantner, S. Mahesh, C. Greenland, J. E. Macdonald, G. Palmisano, H. J. Snaith, D. G. Lidzey, S. D. Stranks, R. H. Friend, and S. Lilliu, "In situ simultaneous photovoltaic and structural evolution of perovskite solar cells during film formation," Energy Environ. Sci. **11**(2), 383–393 (2018).
8. T. Ma, Q. Song, D. Tadaki, M. Niwano, and A. Hirano-Iwata, "Unveil the Full Potential of Integrated-Back-Contact Perovskite Solar Cells Using Numerical Simulation," ACS Appl. Energy Mater. **1**(3), 970–975 (2018).
9. X. Lin, A. N. Jumabekov, N. N. Lal, A. R. Pascoe, D. E. Gómez, N. W. Duffy, A. S. R. Chesman, K. Sears, M. Fournier, Y. Zhang, Q. Bao, Y.-B. Cheng, L. Spiccia, and U. Bach, "Dipole-field-assisted charge extraction in metal-perovskite-metal back-contact solar cells," Nat. Commun. **8**(1), 1–8 (2017).
10. X. Lin, A. S. R. Chesman, S. R. Raga, A. D. Scully, L. Jiang, B. Tan, J. Lu, Y. B. Cheng, and U. Bach, "Effect of Grain Cluster Size on Back-Contact Perovskite Solar Cells," Adv. Funct. Mater. **28**(45), 1–9 (2018).
11. G. D. Tainter, M. T. Hörantner, L. M. Pazos-Outón, R. D. Lamboll, H. Āboliņš, T. Leijtens, S. Mahesh, R. H. Friend, H. J. Snaith, H. J. Joyce, and F. Deschler, "Long-Range Charge Extraction in Back-Contact Perovskite Architectures via Suppressed Recombination," Joule **3**(5), 1301–1313 (2019).
12. G. DeLuca, A. N. Jumabekov, Y. Hu, A. N. Simonov, J. Lu, B. Tan, G. W. P. Adhyaksa, E. C. Garnett, E. Reichmanis, A. S. R. Chesman, and U. Bach, "Transparent Quasi-Interdigitated Electrodes for Semitransparent Perovskite Back-Contact Solar Cells," ACS Appl. Energy Mater. **1**(9), 4473–4478 (2018).
13. H. Seidel, L. Csepregi, A. Heuberger, and H. Baumgartel, "Anisotropic Etching of Crystalline Silicon in Alkaline Solutions," J. Electrochem. Soc. **137**(11), 3612–3626 (1990).
14. Y. Inomata, K. Fukui, and K. Shirasawa, "Surface texturing of large area multicrystalline silicon solar cells using reactive ion etching method," Sol. Energy Mater. Sol. Cells **48**(1-4), 237–242 (1997).

Optics EXPRESS

15. D. H. Macdonald, A. Cuevas, M. J. Kerr, C. Samundsett, D. Ruby, S. Winderbaum, and A. Leo, "Texturing industrial multicrystalline silicon solar cells," Sol. Energy **76**(1-3), 277–283 (2004).
16. M. C. Wei, S. J. Chang, C. Y. Tsia, C. H. Liu, and S. C. Chen, "SiNx deposited by in-line PECVD for multi-crystalline silicon solar cells," Sol. Energy **80**(2), 215–219 (2006).
17. D. Zhang, I. A. Digdaya, R. Santbergen, R. A. C. M. M. van Swaaij, P. Bronsveld, M. Zeman, J. A. M. van Roosmalen, and A. W. Weeber, "Design andfabrication of a SiOx/ITO double-layer anti-reflective coating for heterojunction silicon solar cells," Sol. Energy Mater. Sol. Cells **117**, 132–138 (2013).
18. D. Hocine, M. S. Belkaid, M. Pasquinelli, L. Escoubas, J. J. Simon, G. A. Rivière, and A. Moussi, "Improved efficiency of multicrystalline silicon solar cells by TiO2 anti reflection coatings derived by APCVD process," Mater. Sci. Semicond. Process. **16**(1), 113–117 (2013).
19. M. Lipiński, A. Kaminski, J.-F. Lelièvre, M. Lemiti, E. Fourmond, and P. Zięba, "Investigation of graded index SiOxNy antireflection coating for silicon solar cell manufacturing," Phys. Status Solidi C **4**(4), 1566–1569 (2007).
20. M. Zhang, B. Wilkinson, Y. Liao, J. Zheng, C. F. J. Lau, J. Kim, J. Bing, M. A. Green, S. Huang, and A. W.-Y. Ho-Baillie, "Electrode Design to Overcome Substrate Transparency Limitations for Highly Efficient 1 cm^2 Mesoscopic Perovskite Solar Cells," Joule **2**(12), 2694–2705 (2018).
21. J. Chen, Y. Shen, B. Chen, K. Ge, J. Guo, Z. Wang, F. Li, Y. Xu, and Y. Mai, "Polymer Thin Films for Anti-Reflection and Passivation on the Front Surface of Interdigitated Back Contact c-Si Solar Cell," Sol. RRL **1**, 1700079 (2017).
22. G. Beadie, M. Brindza, R. A. Flynn, A. Rosenberg, and J. S. Shirk, "Refractive index measurements of poly(methyl methacrylate) (PMMA) from 0.4–1.6μm," Appl. Opt. **54**(31), F139–F143 (2015).
23. P. Löper, M. Stuckelberger, B. Niesen, J. Werner, M. Filipič, S. J. Moon, J. H. Yum, M. Topič, S. De Wolf, and C. Ballif, "Complex refractive index spectra of CH3NH3PbI3 perovskite thin films determined by spectroscopic ellipsometry and spectrophotometry," J. Phys. Chem. Lett. **6**(1), 66–71 (2015).
24. H. Yu, F. Wang, F. Xie, W. Li, J. Chen, and N. Zhao, "The role of chlorine in the formation process of CH3NH3PbI3-xClx perovskite," Adv. Funct. Mater. **24**(45), 7102–7108 (2014).
25. T. Dittrich, C. Awino, P. Prajongtat, B. Rech, and M. C. Lux-Steiner, "Temperature Dependence of the Band Gap of CH3NH3PbI3 Stabilized with PMMA: A Modulated Surface Photovoltage Study," J. Phys. Chem. C **119**(42), 23968–23972 (2015).
26. Z. Chu, M. Yang, P. Schulz, D. Wu, X. Ma, E. Seifert, L. Sun, X. Li, K. Zhu, and K. Lai, "Impact of grain boundaries on efficiency and stability of organic-inorganic trihalide perovskites," Nat. Commun. **8**(1), 1–8 (2017).
27. S. N. Habisreutinger, T. Leijtens, G. E. Eperon, S. D. Stranks, R. J. Nicholas, and H. J. Snaith, "Carbon nanotube/polymer composites as a highly stable hole collection layer in perovskite solar cells," Nano Lett. **14**(10), 5561–5568 (2014).
28. T. Leijtens, G. E. Eperon, N. K. Noel, S. N. Habisreutinger, A. Petrozza, and H. J. Snaith, "Stability of Metal Halide Perovskite Solar Cells," Adv. Energy Mater. **5**(20), 1500963 (2015).
29. L. A. A. Pettersson, L. S. Roman, and O. Inganäs, "Modeling photocurrent action spectra of photovoltaic devices based on organic thin films," J. Appl. Phys. **86**(1), 487–496 (1999).
30. P. B. Johnson and R. W. Christy, "Optical constants of the noble metals," Phys. Rev. B **6**(12), 4370–4379 (1972).
31. A. D. Rakić, A. B. Djurišić, J. M. Elazar, and M. L. Majewski, "Optical properties of metallic films for vertical-cavity optoelectronic devices," Appl. Opt. **37**(22), 5271–5283 (1998).
32. I. H. Malitson, "Refraction and Dispersion of Synthetic Sapphire," J. Opt. Soc. Am. **52**(12), 1377–1379 (1962).
33. J. M. Ball, S. D. Stranks, M. T. Hörantner, S. Hüttner, W. Zhang, E. J. W. Crossland, I. Ramirez, M. Riede, M. B. Johnston, R. H. Friend, and H. J. Snaith, "Optical properties and limiting photocurrent of thin-film perovskite solar cells," Energy Environ. Sci. **8**(2), 602–609 (2015).
34. J. R. Devore, "Refractive Indices of Rutile and Sphalerite," J. Opt. Soc. Am. **41**(6), 416–419 (1951).
35. J. Peng, Y. Wu, W. Ye, D. A. Jacobs, H. Shen, X. Fu, Y. Wan, T. Duong, N. Wu, C. Barugkin, H. T. Nguyen, D. Zhong, J. Li, T. Lu, Y. Liu, M. N. Lockrey, K. J. Weber, K. R. Catchpole, and T. P. White, "Interface passivation using ultrathin polymer-fullerene films for high-efficiency perovskite solar cells with negligible hysteresis," Energy Environ. Sci. **10**(8), 1792–1800 (2017).
36. J. Peng, J. I. Khan, W. Liu, E. Ugur, T. Duong, Y. Wu, H. Shen, K. Wang, H. Dang, E. Aydin, X. Yang, Y. Wan, K. J. Weber, K. R. Catchpole, F. Laquai, S. De Wolf, and T. P. White, "A Universal Double-Side Passivation for High Open-Circuit Voltage in Perovskite Solar Cells: Role of Carbonyl Groups in Poly(methyl methacrylate)," Adv. Energy Mater. **8**(30), 1801208 (2018).
37. S.-H. Turren-Cruz, A. Hagfeldt, and M. Saliba, "Methylammonium-free, high-performance, and stable perovskite solar cells on a planar architecture," Science **362**(6413), 449–453 (2018).
38. F. Wang, A. Shimazaki, F. Yang, K. Kanahashi, K. Matsuki, Y. Miyauchi, T. Takenobu, A. Wakamiya, Y. Murata, and K. Matsuda, "Highly Efficient and Stable Perovskite Solar Cells by Interfacial Engineering Using Solution-Processed Polymer Layer," J. Phys. Chem. C **121**(3), 1562–1568 (2017).